This article has been accepted for inclusion in a future issue of this journal. Content is final as presented, with the exception of pagination.

Laser-Powered Co-Firing Process for Highly Efficient Si Solar Cells

Daniel Ourinson, Gernot Emanuel, Kaveh Rahmanpour, Felix Ogiewa, Harald Müller, Eve Krassowski, Hannes Höffler, Florian Clement, and Stefan W. Glunz

***Abstract*—This article presents a successful laser-powered co-firing process for highly efficient Si solar cells as a more compact and energy-efficient alternative to the conventional firing process in an infrared (IR) lamp-powered heat chamber. The best cell group reaches with laser firing only $0.1\%_{\mathrm{abs}}$ lower cell efficiency compared to the best group with conventional firing, demonstrating the industrial potential of this laser firing technology. Adding the laser enhanced contact optimization (LECO) process after firing improves the cell efficiency for laser firing to the level of conventional firing, demonstrating the potential of the combination of the laser firing and the LECO process.**

***Index Terms*—Alternative firing, firing process, laser enhanced contact optimization (LECO), short-circuit effect, silicon solar cells, thermography, vertical cavity surface-emitting laser (VCSEL).**

I. Introduction

The contact firing is a well-established process in the industrial silicon solar cell production [1]. The firing process divides into a low temperature burnout phase, where the binders of the metal pastes burn out, and a high temperature peak phase, where the cell contacts are co-formed on both sides [2]. The industrial firing process (further called "conventional firing") takes place in a conveyor belt furnace, where the wafers are thermally processed in an isolated infrared (IR) lamp-powered chamber. The working principle of this chamber is high air temperature and homogenization of the lamp radiation via reflective walls [1]. The resulting mix of convective and reflective radiative heating leads to a substantial amount of wasted energy that is not heating the wafer—namely the energy needed for heating up the heat chamber and the energy in form of radiation that eventually is not absorbed by the wafer. Low powered industrial IR lamps and the aforementioned energy waste result in low power densities on the wafer. Therefore, long chambers with a large footprint are required to heat the wafer to the necessary temperatures of around 700–900 °C.

This article presents the investigation of an alternative firing process. Based on the work in [3] from 2015, the peak phase is conducted in an alternative firing device instead of the conventional heat chamber, while the burnout phase still remains in the heat chamber. In this alternative peak zone, the wafer is heated by vertical cavity surface-emitting laser (VCSEL) modules [3] (further called "laser firing"). Unlike the conventional IR lamps, the VCSEL modules are area emitters which heat the wafer through direct radiation. Therefore, a higher portion of the emitted radiation can impinge on the wafer, leading to less required output power. While the conventional heat chamber requires high air temperature, the laser radiation manages to heat up the wafer to the necessary peak temperatures while the surrounding air temperature can be kept cold. This way, the power on heating the chamber can be saved. As a result, the laser firing presents a more energy-efficient alternative. Compared to conventional IR lamps, the VCSEL modules enable higher power density emission and, therefore, lead to higher power densities impinging on the wafer. Due to the latter fact, the required footprint of the alternative peak zone becomes substantially lower than for the conventional peak zone. Considering these advantages, this laser peak zone presents an alternative that has the potential of lower production costs while not limiting the throughput compared to conventional firing. The alternative peak zone of this article is an intermediate step towards an even more compact and energy-efficient complete alternative firing equipment featuring area-emitting radiation sources and low ambient air temperature.

In the work of [3], low-efficient aluminum back surface field (Al-BSF) cells [4] were investigated as a proof-of-concept for laser firing. Similar cell efficiencies were reached with the laser firing compared to conventional firing, demonstrating the functionality of this alternative firing process. The aim of the present work is to achieve similar success on higher efficient Si solar cells, such as passivated emitter and rear cells (PERC) [5], especially since the latter replaced Al-BSF cells as the leading market technology in 2019 [6]. An increase in cell efficiency can give rise to performance-limiting effects that are negligible for lower cell efficiencies. Compared to [3], we, therefore, conduct a more detailed investigation of the laser firing process with additional features and approaches, which are presented in the next section.

Manuscript received November 27, 2020; accepted December 4, 2020. This work was supported in part by the German Federal Ministry for Economic Affairs and Energy within the research project "Feuerdrache" under Grant 0324205A. *(Corresponding author: Daniel Ourinson.)*

Daniel Ourinson, Gernot Emanuel, Kaveh Rahmanpour, Hannes Höffler, Florian Clement, and Stefan W. Glunz are with the Fraunhofer Institute for Solar Energy Systems ISE, 79110 Freiburg, Germany (e-mail: daniel.ourinson@ise.fraunhofer.de; gernot.emanuel@ise.fraunhofer.de; kaveh.rahmanpour@ise.fraunhofer.de; hannes.hoeffler@ise.fraunhofer.de; florian.clement@ise.fraunhofer.de; stefan.glunz@ise.fraunhofer.de).

Felix Ogiewa is with Trumpf Photonic Components GmbH, 52074 Aachen, Germany (e-mail: felix.ogiewa@trumpf.com).

Harald Müller is with Rehm Thermal Systems GmbH, 89143 Blaubeuren-Seissen, Germany (e-mail: h.mueller@rehm-group.com).

Eve Krassowski is with CE Cell Engineering GmbH, 06184 Kabelsketal, Germany (e-mail: e.krassowski@cell-engineering.de).

Color versions of one or more of the figures in this article are available at https://doi.org/10.1109/JPHOTOV.2020.3043856.

Digital Object Identifier 10.1109/JPHOTOV.2020.3043856

This article has been accepted for inclusion in a future issue of this journal. Content is final as presented, with the exception of pagination.

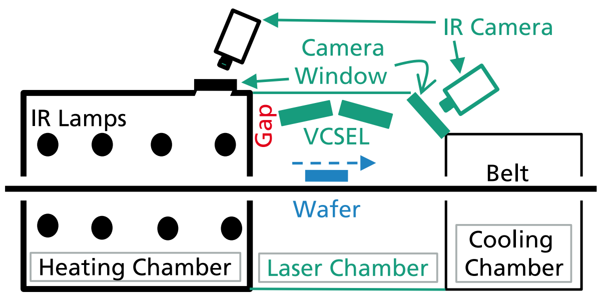

(a)

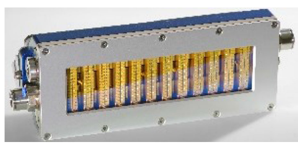

(b)

Fig. 1. (a) lateral scheme of the used inline firing furnace with the integrated laser peak zone (without mirrors–shown in Fig. 3(a) instead). The black color represents the conventional parts of this furnace while the green color shows the novel parts for the laser peak zone. The blue dashed arrow shows the wafer transport direction (b) Image of a VCSEL module (with facing emitting surface), utilized in this work.

II. Experimental

A. Laser Peak Zone and Its Temperature Monitoring

The laser peak zone was integrated in the form of a laser-protected chamber between the heating and cooling chamber of an industry-oriented conveyor belt furnace by *Rehm Thermal Systems* in the PV-TEC laboratory at *Fraunhofer ISE* [see Fig. 1(a)]. Two VCSEL modules by *Trumpf Photonic Components* [see Fig. 1(b)] were installed into the laser chamber above the belt with their beams overlapping and being maximally directed at the passing wafer. A space gap of ca. 15 cm between the heating chamber and the VCSEL modules [see Fig. 1(a)] is unavoidable in the current setup. The emission peak wavelength of the laser is 808 nm, which is well absorbed by Si wafers. The combined maximum output power of both VCSEL modules amounts to 9.6 kW. This leads to maximum power densities of ca. 100 W/cm^2 on the wafer, which is significantly higher than the maximum 20 W/cm^2 in the heating chamber equipped with the present IR lamps. The laser power densities are well sufficient to (quickly) heat a wafer to the required peak temperatures. Regarding the vertical temperature distribution, a simplified 1-D numerical simulation of the temperature diffusion across the wafer depth using the heat equation [7], a c-Si thermal diffusivity of 0.9 cm^2/s [7], a (typical) 180 μm thick Cz-Si wafer, and a 1 μm spatial and 1 ns temporal resolution, reveals that a surface temperature of 800 °C (typical firing temperature), which is kept temporally constant at that surface (serving as a boundary condition and a simple one-sided surface heating), propagates to the opposite surface (which is initially at room temperature) within approximately 1 ms, leading to a homogenous depth distribution at 800 °C. Since significantly longer heating times in the range of seconds take place during firing [see Fig. 3(b)] it is fair to assume homogenous temperature distribution for a one-sided illumination by the laser here, which is why a one-sided illumination is sufficient in this case.

Furthermore, each VCSEL module consists of 24 independently controllable segments, which emit a beam with 5° half angle. The active area of one VCSEL module is 160 × 40 mm. Its longer side is positioned perpendicularly to the wafer transport direction. This way, a standard 156.75 × 156.75 mm-sized wafer is fully illuminated in this direction. In transport direction, the laser illuminates the wafer just locally, but reaches each spot of the wafer during its passing. This way the illumination geometry in the laser peak zone differs from the homogeneous illumination in the conventional peak zone. Highly reflective mirrors are installed left and right to the passing wafer parallel to the transport direction [see Fig. 3(a)]. The mirrors have the purpose to redirect the laser beam falling beyond the wafer back to the wafer, and, thus, to maximize the laser radiation portion impinging on the wafer. For the present equipment, the active part of the laser peak zone in transport direction, i.e., the total length from one end of the double module to the other, is 18 cm long while the peak zone part of the conventional heat chamber is 40 cm long. Thus, the laser peak zone has a lower footprint than the conventional peak zone.

To establish a successful laser firing process, the wafer temperature must be monitored. Classic thermocouple measurements [2], as conducted in [3], cannot be realized in the laser peak zone because the installed mirrors leave no space for the thermocouple equipment to pass. Therefore—based on our previous works in [8] and [9] for conventional firing—an inline infrared (IR) camera by *InfraTec* has been installed outside of the laser chamber [see Fig. 1(a)]. The camera has a detection wavelength range far from the laser emission wavelength range. A camera field of view of the passing wafer is created by a special window that transmits photons in the camera detection wavelength range but shields photons in the laser emission range. Contrary to the local temperature monitoring in [3], the IR camera features *in situ* spatially-resolved measurements, allowing for a more detailed process optimization of the laser peak zone. We use our numerical script from [9] to track each wafer spot of the recorded thermography sequences like "virtual thermocouples." This way, time-temperature profiles of the peak phase including the peak temperature can be plotted for any wafer spot in the laser peak zone, making classic thermocouple measurements unnecessary. Furthermore, the script allows the mapping of the extracted peak temperature from each wafer spot into a 2-D distribution. This way, the spatial temperature distribution can be evaluated. With the help of the presented temperature monitoring, the temperature characteristics during the laser firing are compared to those of the conventional firing from [8].

B. Investigated Solar Cells and Process Flow

Industrial Czochralsky-grown (Cz) monofacial and bifacial *p*-type PERC cells are investigated in this article. Fig. 2 shows the process flow of this article.

For the monofacial cells, the Ag front side grid shape is varied between a: standard H-pattern grid - further called "busbar grid"; grid with fingers only and no redundancy line - further called "busbar-less grid"; and grid consisting of local isolated H-pattern islands by having twelve homogenously distributed interruptions (gap equal to finger spacing) at each

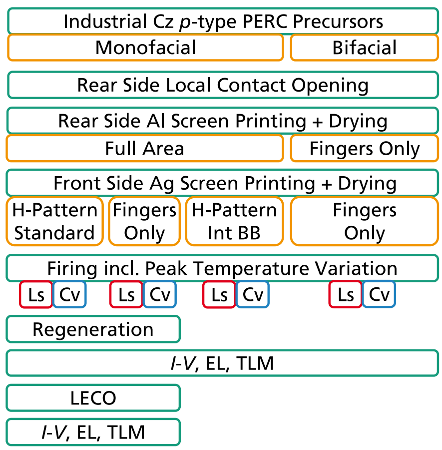

Fig. 2. Schematic process flow of this article. It has to be noted that a different precursor type is used for the LECO-processed cells with busbars. Abbreviations: Int = Interrupted; BB = busbars; Cv = conventional; and Ls = laser.

busbar and redundancy line—further called "interrupted busbar grid." For both sides of the bifacial cells, busbar-less grids are utilized.

A variation of the firing peak temperature is performed with three wafers per temperature for laser and conventional firing, respectively. It is ensured to cover the peak temperature range that respectively includes the best cell performance, which is presented in Section III-C. Thermocouples measure the entire temperature profile for conventional firing and the burnout profile of the laser firing. The latter profile is adapted to the burnout profile of conventional firing while the burnout zone is maximally shifted to the end of the heat chamber. The IR camera introduced in Section II-A measures the peak zone profile of the laser firing.

Current-Voltage (*I*–*V*) measurements and electroluminescence (EL) imaging [10] are conducted for fired cells. From the *I*–*V* measurements, the cell efficiency (η), open-circuit voltage ($V_{\rm OC}$), short-circuit current density ($j_{\rm SC}$), fill factor (FF), pseudo FF (pFF), ideal FF (FF_0), shunt resistance, as well as front and rear side lateral (grid) resistance are extracted. From each cell group, the cell with the pFF-FF value closest to that of the group's average pFF-FF value is chosen for transfer length method (TLM) measurements to determine the spatially averaged contact resistivity. The shunt losses of a cell are characterized by the shunt resistance and the FF_0-pFF value. The contact sintering quality of both sides during firing is investigated by the lateral resistances. The optical losses are analyzed by the $j_{\rm SC}$. The resistive losses are investigated by the pFF-FF value [11], the contact resistivity, and the EL images. The recombinative losses in the emitter and bulk of the cell are investigated by the $V_{\rm OC}$ while these losses in the space charge region are analyzed by the FF_0-pFF value [11].

In addition to sole laser firing, its combination with *Cell Engineering*'s innovative "laser enhanced contact optimization" (LECO) process [12], [13] is investigated for monofacial cells with and without busbars. As the cells were transported between *ISE* and *Cell Engineering*, the cells were stabilized after firing by regeneration regarding light induced degradation [14]. The LECO process improves underfired Ag contacts to the state of optimally fired contacts by simultaneous local laser illumination and electric treatment (contrary to thermal treatment during firing). *Cell Engineering*'s original aim is to combine the LECO process with conventional firing for various applications such as sharpening the efficiency distribution towards a higher yield as well as increasing process windows with standard pastes, and achieving higher cell efficiencies with special LECO-adapted pastes [13]. Due to IP agreements, the LECO process is not presented in more detail.

III. Results and Discussion

A. *Wafer Temperature Evaluation During Laser Firing*

In this article, the cell performance depends significantly on the wafer temperature during firing [see Section III-C-D]. Therefore, the temperature results are presented prior to the cell performance results. Representatively for all investigated wafers, Fig. 3 demonstrates the temperature results on one wafer from each of the respective best efficient groups of the monofacial busbar-less cells.

Fig. 3(a) shows a thermography snapshot of the wafer passing through the laser peak zone, demonstrating the successful spatial temperature monitoring during the laser firing. One can observe that the laser contemporaneously illuminates ca. one third of the wafer in transport direction.

Fig. 3(b) shows the time-temperature profile during the laser firing in comparison to conventional firing. While the laser firing profile turns out similar to the conventional profile for the most part, the former differs by a temperature drop between the burnout and peak phase, like in the case of [3]. This drop stems from the previously mentioned space gap between the heating chamber and the laser modules in the realized setup of this equipment. As a wafer is transported during the firing process, there is a local time shift of the wafer heating in transport direction, leading to contemporaneous wafer temperature inhomogeneity in transport direction. The above-mentioned drop can lead - in combination with the local laser heating - to a significantly higher contemporaneous temperature inhomogeneity before as well as during the peak phase [cf. Fig. 3(a)] and a more pronounced local time shift in heating in transport direction compared to the conventional firing.

Not to be confused with the previously mentioned contemporaneous temperature distribution, Fig. 3(c) shows the 2-D peak temperature mapping for the laser firing, which is compared to conventional firing (for the latter, discussion of results in [8]. It is clearly visible that the laser-fired wafer experiences a significantly higher spatial temperature inhomogeneity than the conventionally fired wafer. The separation of the two-dimensional temperature distribution into the averaged 1-D distributions in and perpendicular to the transport direction [9] [see Fig. 3(d)] reveals the origin of the higher inhomogeneity for laser firing. While the temperature distribution in transport direction is similar for both firing methods, the laser-fired inhomogeneous distribution perpendicular to the transport direction reveals itself to be the cause of the overall inhomogeneity.

The observed sinusoidal shape of the temperature distribution perpendicular to the transport direction can be explained in the following way. During the firing process, a wafer naturally experiences an increased convective temperature loss at the wafer edges. The higher the difference between the wafer and the surrounding air temperature, the higher these convective losses. In the case of the conventional heat chamber, this difference is

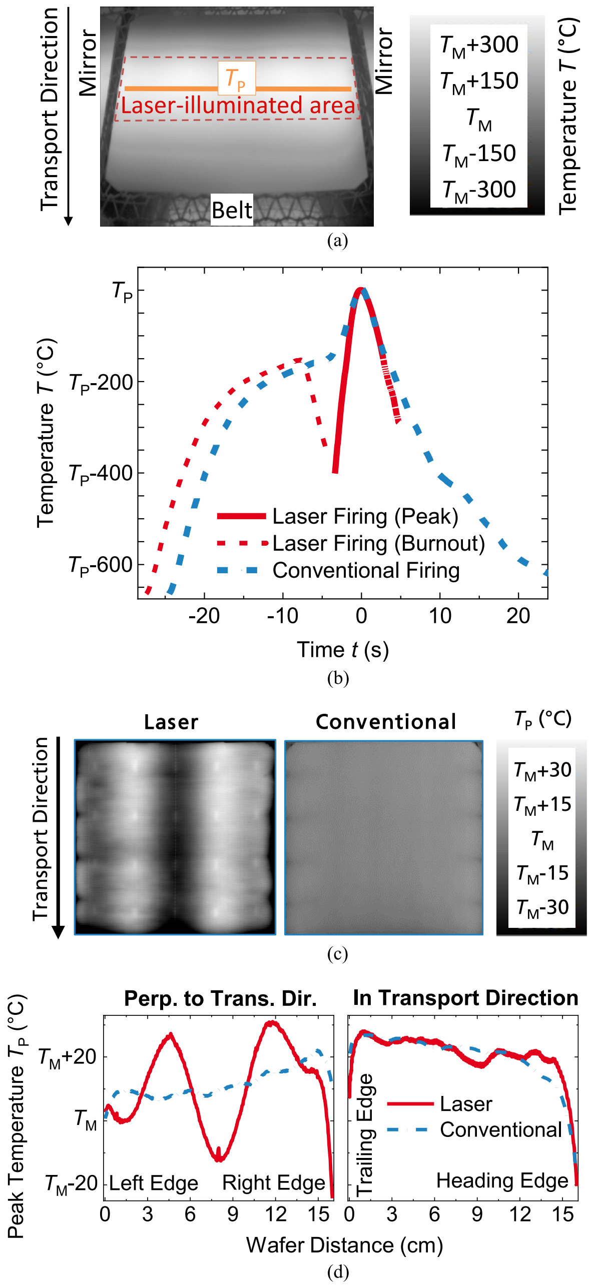

Fig. 3. (a) Representative snapshot of a laser-heated wafer passing the laser peak zone. The orange solid line represents the region of the peak temperature. (b) Representative time-temperature profiles (locally at the wafer center) for conventional and laser firing. The thermocouple-measured burnout profile for laser firing is only shown until the point where the thermography-measured peak profile starts. (c) Spatial 2-D wafer peak temperature mapping for conventional [9] and laser firing from (b). (d) Averaged one-dimensional distributions in both wafer directions from (c). Abbreviations: T_P = peak temperature; T_M = arbitrary middle temperature in an axis/legend; and "Perp. to Trans. Dir." = perpendicular to transport direction.

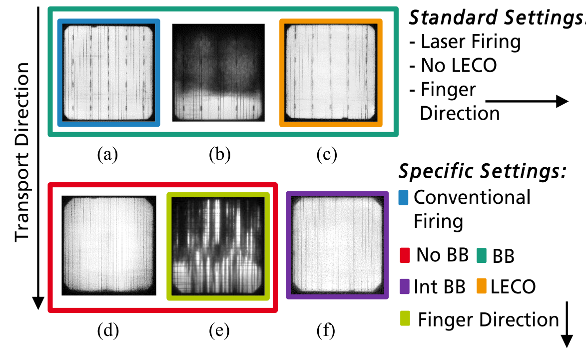

Fig. 4. Representative EL images for the relevant cell groups. By default, the defined "standard settings" apply to the EL images. In case other settings do apply, the latter are pointed out as "specific settings" in the form of a specific color outline.

relatively small and results in a relatively small temperature drop at the wafer edges [8]. In the case of the laser peak zone, the air temperature is relatively cold, which results in a relatively high temperature drop at the wafer edges. In addition to the convective losses, the active length of the VCSEL modules perpendicular to the transport direction of 160 mm is similar to the length of a standard 156.75 × 156.75 mm-sized wafer. This results in lower radiation power densities at the wafer edges due to the cone shaped laser beam. The installed mirrors help to reduce the temperature edge drop significantly but cannot mitigate this obstacle entirely. In addition to the mirrors, the independent power control of each VCSEL segment allows the creation of intentional spatial gradients of the emitted power density. First, the power density at the wafer edges is increased. This reduces the edge temperature drop further but cannot eliminate the latter, either. In the same time, the increase of the edge power density heats up the areas toward the wafer center as well. To compensate for the latter heating while simultaneously not increasing the edge drop, the best-obtained compromise is to reduce the temperature at the wafer center, leading to the observed sinusoidal shape. The asymmetric distribution is assumed to stem from possible asymmetric (cool) airflow in the laser chamber. This temperature shape features the most homogeneous distribution for laser firing achieved so far. On a positive note, these distribution characteristics are reproducible for various firing conditions.

B. *Suspected Short-Circuit Effect for Laser-Fired Cells*

In this article, we observe a characteristic distribution of the EL signal for laser-fired cells with a standard Ag H-pattern grid: A higher signal (assuming good contact formation) at the heading parts and a lower signal (assuming bad contact formation) at the trailing parts during firing [see Fig. 4(b)]. We believe that this EL pattern might stem from the "short-circuit effect" described by Kim *et al.* [15]: direct ("short-circuited") Si-Ag(bulk) connections that supposedly cause a lack of emitter electrons leading to fewer Ag crystallites and an effectively underfired contact. These "Ag-Si short-circuits" form locally and nonuniformly, and are caused by non-uniformities, such as the locally time-shifted wafer heating in transport direction (see Section III-A) and the resulting time-shifted contact formation process [16], [17]. These "Ag-Si short-circuits" supposedly only affect grid parts which are connected to these spots, but not parts which are disconnected. This effect is believed to strongly affect the cell performance in this work (see Section III-C) which is why the mentioned characteristic EL response and the suspected short-circuit effect need to be discussed prior to the cell performance results in the following.

The observations and assumptions made in [15]–[17] apply to the EL pattern of the laser-fired cell with the H-pattern grid in Fig. 4(b). Due to the locally time-shifted contact formation process, the heading parts are assumed to form the short-circuit spots first, but most likely also complete the contact formation process earlier than the trailing parts which is why the heading parts probably still “have time” to form a proper amount of Ag crystallites leading to good contact formation and higher EL signal. On the contrary, the trailing parts do not have that time, leading to bad contact formation and lower EL signal. Following the example of Chu *et al.* [16], the replacement of the H-pattern grid by a busbar-less grid with the fingers fired perpendicularly to the transport direction does lead to a higher EL signal at the trailing cell parts being at the same level as for the heading cell parts [see Fig. 4(d)], being comparable to the positive effect observed in [16]. This suggests a significant reduction of the short-circuit effect to a negligible level. However, when firing the fingers in transport direction (which is usually not done), the suspected short-circuit effect does emerge [see Fig. 4(e)], as in the case of the H-pattern grid. In accordance with the explanations in [15]–[17], this result suggests that grid interruptions in transport direction lead to a reduction of the short-circuit effect while a connected grid in transport direction—even with interruptions perpendicular to the transport direction— still shows the short-circuit effect. Furthermore, a much lower amount of grid interruptions in transport direction than in the case of the busbar-less grid—here for an H-pattern grid with homogenously interrupted busbars—seems to be sufficient to decrease the short-circuit effect, as well [see Fig. 4(f)]. While the laser-fired cells with (uninterrupted) busbars clearly indicate the short-circuit effect, the conventionally fired cells with the same grid do not—at least being not observable [see Fig. 4(a)]. The possible reasons why the conventionally fired cells of [15], [16] do show signs of the short-circuit effect (contrary to our conventionally fired cells), could be the utilization of special test structures [15] or different cell types with different properties such as sheet resistances or surface morphologies [16] (compared to the present work). In accordance, different cell configurations in [16] show lower or higher amount of the suspected short-circuit effect, suggesting that different combinations affect the previously mentioned local contact nonuniformities differently. When comparing our conventionally fired to the laser-fired cells, one parameter, which also can contribute to local contact nonuniformities, differs significantly—namely temperature -, as previously elaborated in Section III-A. On account of the significantly higher contemporaneous wafer temperature inhomogeneity in transport direction for the laser firing and the correspondingly assumed significantly more pronounced local time shift of the contact formation process, we assume that the short-circuit effect is stronger pronounced for the laser firing than for the conventional firing.

C. Cell Performance Results Without LECO Process

As obtained from Section III.A-B, the cells show differences for both firing methods. Despite that, certain electric characteristics turn out similar after laser firing compared to conventional firing, being typical for well-processed cells, within the same cell configuration. The lateral resistances are comparable, which indicates similar sintering quality during firing. The FF_0-pFF values are resembling, which implies similar recombinative losses in the space charge region and the absence of shunt problems. The j_{SC} is (with one later explained exception) similar, which suggests similar optical properties (see Table I). Unlike the previously mentioned parameters, the V_{OC} [see Fig. 5(c)], pFF-FF [see Fig. 5(b)] and cell efficiency [see Fig. 5(a)], in turn, show clear differences for both firing methods.

TABLE I

FURTHER *I–V* RESULTS AND CONTACT RESISTIVITY FOR COMPLETING THE DATA SET WITH RESPECT TO FIG. 5. THE STANDARD DEVIATION FOR THE CONTACT RESISTIVITY REFERS TO THE SPATIAL DEVIATION OF THE RESPECTIVE CELL

	Monofacial						Bifacial	
	BB		Int BB		No BB			
	Ls	Cv	Ls	Cv	Ls	Cv	Ls	Cv
j_{SC} (mA/cm^2)	39.8 ±0.2	40.1 ±0.1	39.6 ±0.1	39.6 ±0.0	40.4 ±0.0	40.3 ±0.1	39.9 ±0.1	39.9 ±0.0
FF (%)	76.4 ±0.7	81.2 ±0.1	80.6 ±0.1	80.8 ±0.1	80.5 ±0.1	81.2 ±0.3	80.1 ±0.1	80.6 ±0.0
pFF (%)	82.3 ±0.4	83.3 ±0.2	82.9 ±0.1	82.9 ±0.1	83.1 ±0.1	83.0 ±0.1	82.8 ±0.1	82.7 ±0.0
ρ_{C} (mΩ cm^2)	34.4 ± 14.4	1.3± 0.4	1.7± 0.6	1.4± 0.4	2.2± 0.6	1.2± 0.3	3.3 ±2.7 (FS) 1.0 ±0.2 (RS)	0.9 ±0.3 (FS) 0.9 ±0.1 (RS)

Abbreviations: FS = front side; RS = rear side.

The suspected short-circuit effect (see Section III-B) for laser-fired cells with a standard H-pattern grid causes bad contact formation for a large area of the corresponding monofacial PERC cells [see Fig. 4(b)]. This results in significantly higher resistive losses compared to conventional firing, as can be obtained from the pFF-FF values. A similar trend can be seen in the contact resistivity values (see Table I). On that note, the trend of the latter is similar to the that of the overall resistive losses for all cell configurations of this work. This makes sense since the lateral resistance is similar for both firing methods, as previously mentioned. Thus, the overall resistive losses are most likely originating from the resistive losses at the contacts. Furthermore, the impact of the suspected short-circuit effect varies with each cell [see high standard deviation in Fig. 5(b)], leading to irreproducible characteristics of the same firing processes. Apart from a minor contribution of the lower V_{OC}, the resistive losses are responsible for the lion share of the resulting $1.6\%_{\mathrm{abs}}$ cell efficiency gap to conventionally fired cells. On that note, the observable j_{SC} loss stems from the heavy resistive losses, as well.

As discussed in Section III-B, the suspected short-circuit effect in case of the laser firing can be mitigated by Ag grid designs with interrupted or without busbars [see Fig. 4(d) and (f)]. This results in significantly lower resistive losses for the corresponding monofacial and bifacial PERC cells. This, in turn, leads to a reduction of the efficiency gap to $0.1\%_{\mathrm{abs}}$ for busbar-less monofacial, $0.25\%_{\mathrm{abs}}$ for busbar-less bifacial and $0.2\%_{\mathrm{abs}}$ for monofacial cells with interrupted busbars, respectively. The

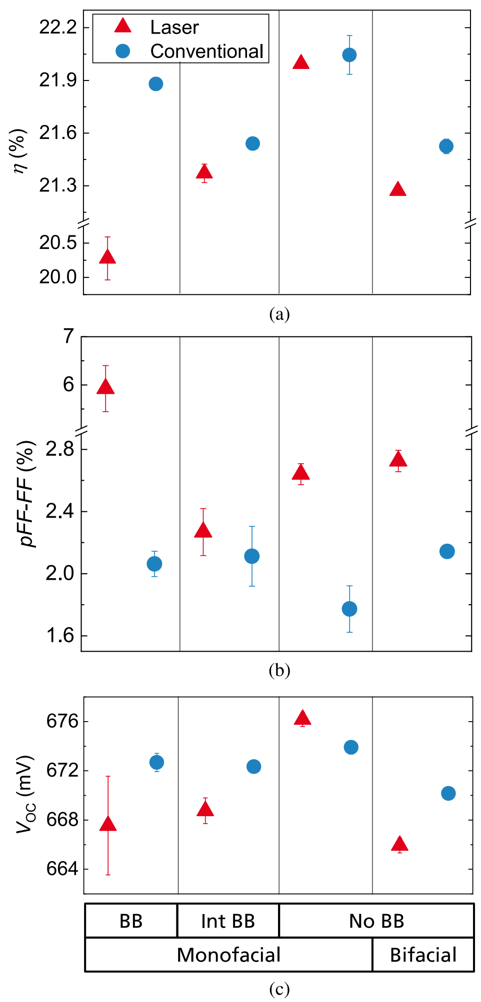

Fig. 5. *I–V* results for the respective most efficient (LECO-free) cell groups (three wafers per group) from the respective peak temperature variations (see Section II-B). The efficiency for cells with interrupted busbars is lower due to the utilization of a front side grid with more fingers (originally designed for rear side applications) than for the grids with and without busbars, leading to lower j_{SC} (see Table I). All the cells are fired with the fingers perpendicular to the transport direction.

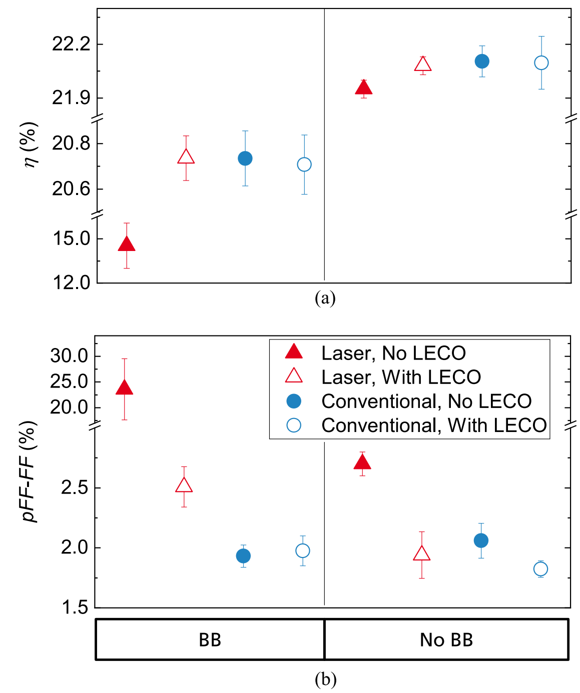

Fig. 6. *I–V* results for LECO-processed cell groups (three wafers per group).

remaining efficiency gaps stem from the remaining slightly higher resistive and/or recombinative losses. It is very likely, that the higher spatial wafer temperature inhomogeneity presented in Section III-A causes the presence of both under- and/or overfired areas on the same cell, leading to the observed resistive and recombinative losses, resulting in lower cell efficiencies. The difference in these remaining losses is most likely determined by the ratio of the spatial wafer temperature inhomogeneity to the optimum firing temperature range for a specific cell configuration.

Compared to the work in [3], the efficiency gap between the laser and conventional firing cannot be closed entirely, on the one hand. On the other hand, the assumed responsible obstacles, namely the suspected short-circuit effect and the temperature inhomogeneity, were not investigated in [3], which might have been present but negligible for the investigated low-efficient cells.

Representatively for all cell configurations, the firing settings of the monofacial busbar-less cells of Fig. 5 are chosen to determine the required output power for the different peak zones. For laser firing, the total output power of both VCSEL modules amounts to 1960 W. For conventional firing, the IR lamps which are responsible for the peak phase yield a combined output power of 3200 W. Hence, this result indicates a 40% lower power output for the laser firing.

D. Cell Performance Results With LECO Process

Since the laser firing related performance losses presented in Section III-C stem mainly from locally underfired Ag contacts, one way to improve the latter is to apply the LECO process after the firing step. Accordingly, the resistive losses due to underfired cell parts originating from the inhomogeneous laser firing are significantly reduced for the monofacial busbar-less cells [see Fig. 6(b)]. Furthermore, the resistive losses due to the underfired cell parts originating from the suspected short-circuit effect are substantially reduced for the monofacial cells with the standard busbar grid.

In accordance, the LECO process increases the low signal of the trailing parts in the EL image of the laser-fired busbar cell depicted in Fig. 4(b) to the level of the heading parts, which is shown in Fig. 4(c). These optimizations (and a slightly higher V_{OC}, see Table II) improve the cell efficiency for the laser-fired cells of both types to the level of the respective conventionally fired cells [see Fig. 6(a)], closing the corresponding remaining efficiency gaps presented in Section III-C. It has to be noted that the efficiency level of the busbar cells here is ca. $0.5\%_{\text{abs}}$ lower than usual, on account of an unsuited regeneration process. However, this circumstance is regarded as uncritical, since the main objective here is to demonstrate the compensation of the

TABLE II
FURTHER *I–V* RESULTS AND CONTACT RESISTIVITY FOR COMPLETING THE DATA SET WITH RESPECT TO FIG. 6

	BB				No BB			
	Before LECO		After LECO		Before LECO		After LECO	
	Ls	Cv	Ls	Cv	Ls	Cv	Ls	Cv
j_{SC} (mA/cm^2)	37.5 ±11	39.4 ±0.1	39.5 ±0.1	39.4 ±0.0	40.4 0.1±	40.4 ±0.1	40.4 0.1±	40.4 ±0.1
V_{OC} (mV)	658 ±1.5	657 ±1.6	659 ±1.1	657 ±1.0	675 ±1.0	675 ±0.9	675 ±1.3	675 ±1.2
FF **(%)**	58.7 ±5.8	80.0 ±0.3	79.7 ±0.2	79.9 ±0.4	80.5 ±0.3	81.0 ±0.2	81.0 ±0.2	81.1 ±0.2
pFF **(%)**	82.3 ±0.2	81.9 ±0.4	82.2 ±0.2	81.9 ±0.5	83.2 ±0.1	83.1 ±0.2	82.9 ±0.2	83.0 ±0.3
ρ_C (mΩ cm^2)	172 ±72	1.3 ±0.5	1.7 ±0.2	1.1 ±0.2	2.3 ±0.6	1.3 ±0.5	1.4 ±0.6	1.3 ±0.5

obstacles from the temperature inhomogeneity and the suspected short-circuit effect by the LECO process.

IV. SUMMARY, CONCLUSION, AND OUTLOOK

This work presents the successful contact firing of monofacial and bifacial highly efficient Si solar cells with a more compact and energy-efficient alternative process based on the work of [3] for low-efficient Al-BSF cells. This firing process features an alternative peak zone where the wafer is directly heated by an area-emitting radiation source, namely a VCSEL laser, in a cold surrounding ("laser firing") instead of conventional IR lamps in a heated chamber ("conventional firing"). Therefore, this laser peak zone allows for a smaller footprint and a lower power consumption, decreasing the process costs during firing. Here, the laser peak zone requires ca. 40% less output power than the conventional peak zone. This alternative peak zone is an intermediate step towards an even more compact and energy-efficient complete alternative firing equipment, including the burnout zone.

Compared to conventional firing, the laser firing seems to cause a severe "short-circuit effect" [15] for PERC cells with standard H-pattern Ag grids due to the present setup of the laser peak zone, leading to $1.6\%_{\mathrm{abs}}$ lower cell efficiency. However, this obstacle can be mitigated by busbar-less grids, reducing the efficiency gaps to $0.1\%_{\mathrm{abs}}$ for monofacial and $0.25\%_{\mathrm{abs}}$ for bifacial cells. The remaining gaps stem most likely from simultaneous under- and overfiring due to the higher spatial wafer temperature inhomogeneity in the laser peak zone, monitored by a thermography camera. An optimization of the setup will most likely lead to a better temperature homogeneity and the mitigation of the suspected short-circuit effect. Despite the latter, the small remaining efficiency gaps show the industrial potential of laser firing as an alternative to conventional firing. Since Ag grids with busbars presently seem to cause the short-circuit effect and grids without busbars prevent the conventional busbar-to-busbar module interconnection, both obstacles can be mitigated by the presented grid with interrupted busbars, leading to an efficiency gap of $0.2\%_{\mathrm{abs}}$, which is comparable to the efficiency gaps of the previously mentioned grid designs. The negative effects caused by the suspected short-circuit effect and the temperature inhomogeneity can be healed by adding the LECO process after firing. As a result, the LECO process improves the laser-fired monofacial cells with and without busbars to the performance level after conventional firing, in this work. Thus, apart from the original aim of combining the LECO process with conventional firing—the combination of the LECO process with the laser firing is promising, as well. Apart from solar cells, such an alternative firing technology could be applied for other fields with similar thermal treatment.

ACKNOWLEDGMENT

The authors would like to thank Tayyab Javaid, Tobias Fellmeth, the ISE cell tester and screen printing teams, and all the colleagues who contributed to this work, despite the time of the Covid-19 pandemic.

REFERENCES

[1] J. Xu, J. Zhang, and K., and Kuang, *Conveyor Belt Furnace Thermal Processing*. Heidelberg, Germany: Springer, 2018.
[2] D. Ourinson, G. Emanuel, A. Lorenz, F. Clement, and S. W. Glunz, "Evaluation of the burnout phase of the contact firing process for industrial PERC," in *Proc. AIP Conf.*, 2019, pp. 1–8.
[3] A. Pruijmboom *et al.*, "VCSEL arrays expanding the range of high-power laser systems and applications," *J. Laser Appl.*, vol. 9348, pp. 1–8, 2015.
[4] M. Rauer, C. Schmiga, J. Krause, R. Woehl, M. Hermle, and S. W. Glunz, "Further analysis of aluminum alloying for the formation of p+ regions in silicon solar cells," *Energy Procedia*, vol. 8, pp. 200–206, 2011.
[5] A. W. Blakers, A. Wang, A. M. Milne, J. Zhao, and M. A. Green, "22.8% efficient silicon solar cell," *Appl. Phys. Lett.*, vol. 55, no. 13, pp. 1363–1365, 1989.
[6] VDMA, "International technology roadmap for photovoltaic (ITRPV): 2019 results," VDMA, Frankfurt, Germany2020.
[7] C. Huang, *Heat Transfer in Silicon – Experiments and Simulation*: Thesis, 2016.
[8] D. Ourinson *et al.*, "In situ solar wafer temperature measurement during firing process via inline IR thermography," *Phys. Status Solidi RRL*, vol. 13, no. 10, 2019, Art. no. 1900270.
[9] D. Ourinson, G. Emanuel, G. Dammaß, H. Müller, F. Clement, and S. W. Glunz, "In situ surface temperature measurement in a conveyor belt furnace via inline infrared thermography," *J. Visualized Experiments*, no. 159, pp. 1–7, 2020.
[10] H. Höffler, J. Haunschild, and S. Rein, "Influence of external contacting on electroluminescence and fill factor measurements," *Sol. Energy Mater. Sol. Cells*, vol. 152, pp. 180–186, 2016.
[11] J. Greulich, M. Glatthaar, and S. Rein, "Fill factor analysis of solar cells' current-voltage curves," *Prog. Photovolt., Res. Appl.*, vol. 18, no. 7, pp. 511–515, 2010.
[12] R. Mayberry, K. Myers, V. Chandrasekaran, A. Henning, H. Zhao, and E. Hofmüller, "Laser enhanced contact optimization (LECO) and LECO-Specific pastes: A novel technology for improved cell efficiency," in *Proc 36th Photovol. Conf.*, 2019.
[13] E. Krassowski, S. Großer, M. Turek, and H. Höffler, "Laser enhanced contact optimization a novel technology for metal-semiconductor-contact optimization for crystalline silicon solar cells," in *Proc. 37th Photovolt. Conf. Proc., Online-Conf.*, 2020.
[14] T. Niewelt, J. Schon, W. Warta, S. W. Glunz, and M. C. Schubert, "Degradation of crystalline silicon due to boron–oxygen defects," *IEEE J. Photovolt.*, vol. 7, no. 1, pp. 383–398, 2017.
[15] H.-S. Kim *et al.*, "Electrochemical nature of contact firing reactions for screen-printed silicon solar cells: Origin of "gray finger," phenomenon," *Prog. Photovolt., Res. Appl.*, vol. 24, no. 9, pp. 1237–1250, 2016.
[16] H. Chu *et al.*, "Impact of the presence of busbars during the fast firing process on contact resistances," *IEEE J. Photovolt.*, vol. 8, no. 4, pp. 923–929, Jul. 2018.
[17] H. Chu, Z.-W. Peng, and V. D. Mihailetchi, "A study of the "short-circuit," effect during the fast firing process," in *Proc. 8th in Metallization Interconnection Workshop*, 2019.